ELSEVIER

Journal of Photochemistry and Photobiology A: Chemistry 145 (2001) 173–181

Journal of Photochemistry and Photobiology A:Chemistry

www.elsevier.com/locate/jphotochem

The role of the photochemical fragmentation in laser ablation: a molecular dynamics study

Yaroslava G. Yingling [a], Leonid V. Zhigilei [b], Barbara J. Garrison [a,*]

[a] *Department of Chemistry, 152 Davey Laboratory, The Pennsylvania State University, University Park, PA 16802, USA*
[b] *Department of Materials Science and Engineering, 116 Engineer's Way, University of Virginia, Charlottesville, VA 22904, USA*

Received 10 March 2001; accepted 22 May 2001

Abstract

Despite numerous studies, the mechanistic understanding of the role of the photochemical processes and their coupling with the thermal processes in UV laser ablation is still far from being complete. In this work, the effects of the photochemical reactions on the laser ablation mechanism are delineated based on the results of molecular dynamics simulations of 248 nm laser irradiation of solid chlorobenzene. Photochemical reactions are found to release additional energy into the irradiated sample and decrease the average cohesive energy, therefore decreasing the value of the ablation threshold. The yield of emitted fragments becomes significant only above the ablation threshold. Below the ablation threshold only the most volatile photoproduct, HCl, is ejected in very small amounts, whereas the remainder of photoproducts are trapped inside the sample. Results of the simulations are in a good qualitative agreement with experimental data on the ejection of photoproducts in the laser ablation of chlorobenzene.

Keywords: Photochemical fragmentation; Laser ablation; Molecular dynamics

1. Introduction

Ultraviolet (UV) laser ablation of various molecular materials has raised considerable interest due to its numerous applications in laser surgery and mass analysis of high-weight biological molecules. UV laser irradiation leads to the electronic excitations of the absorbing molecules. An excited molecule can either photochemically decompose or undergo internal conversion to a vibrationally excited ground state, which can then release its energy thermally. It is generally accepted that when photochemical processes occur, thermal processes are also involved.

To understand the role of the photochemical process in laser ablation, extensive experimental studies have been performed. Tsuboi et al. [1,2] have reported on 248 nm laser ablation of liquid benzene and benzene derivatives such as toluene, benzyl chloride, chlorobenzene and benzyl alcohol. Based on the values of temperature estimated for the threshold fluence, they concluded that the ablation of benzene is induced by explosive boiling of the overheated liquid. For the benzene derivatives, however, the estimated sample temperature at threshold did not reach the boiling point, which suggests that thermal processes alone could not be responsible for the ablation onset and the ablation could be triggered by photochemical processes. The ablation threshold was correlated to the photochemical reactivities of the derivatives. Formation of photoproducts in laser ablation of liquid benzene by a 248 and 308 nm pulses was observed by Srinivasan and Ghosh [3] and ascribed to the photochemical decomposition following two-photon absorption. On the other hand, in the investigation of the ablation of a benzene film with the same wavelength, 248 nm, Buck and Hess [4] pointed out the importance of thermal processes. It has been noticed in a number of studies of laser ablation of molecular films that molecular photolysis yields are unexpectedly low under explosive desorption conditions. For example, in the 308 nm laser irradiation of CH_2I_2 films adsorbed on Al_2O_3 and Ag surfaces, the quantum yields of the photodissociation of the parent molecule were found to be much lower than that in the gas phase [5]. Similarly, in the ablation of Cl_2 films at 193 nm, less than 7% of the desorbed species was detected as Cl fragments [6]. In studies of the ablation of ICl [7], XeF_2 [8] and C_6H_5Cl [9] films, a significant amount of new products were observed and attributed to recombination of photofragments. It was suggested that a percentage of the liberated fragments recombine or react to reform the parent molecule, thereby at least partly accounting for the strong parent peak observed under ablation conditions. Despite a considerable number of experimental studies, a detailed

* Corresponding author. Tel.: +1-814-863-5319; fax: +1-814-863-2103.
E-mail address: bjg@chem.psu.edu (B.J. Garrison).

1010-6030/01/$ – see front matter
PII: S1010-6030(01)00580-9

understanding of photochemical processes and their role in the mechanism of laser ablation has not yet emerged.

Molecular dynamics (MD) simulations are utilized in this work to study in detail the photochemical aspects of laser ablation. We chose chlorobenzene as our basic system to model photochemical events because of its well-known gas-phase and solution chemistry. Photofragmentation of chlorobenzene occurs exclusively by scission of the C–Cl bond to yield C_6H_5 and Cl radicals, which in solution and static gas cell experiments react with the precursor molecules to form a number of different products [10]. The photochemistry of C_6H_5Cl has been investigated by numerous experimental techniques [1,2,9,11–14,25]. Using a C_6H_5Cl molecular beam [13], it was found that excitation of chlorobenzene by 248 nm laser light can lead to either photochemical dissociation or vibrational relaxation. It was determined that 36% of the excited molecules are photofragmented with available energy for photofragments of 19 kcal/mol. The ablation of liquid chlorobenzene at the same wavelength has also been investigated by photoacoustic measurements [2]. Two breakpoints were clearly observed in the dependence of photoacoustic signals on laser fluence. For chlorobenzene, the value of the first breakpoint, 60 mJ/cm^2, is in a good agreement with the ablation threshold fluence. The origin of the second breakpoint is not clear. In the ablation of neat C_6H_5Cl films [9,14,25] two fluence ranges were found in which the photolysis of chlorobenzene produces very different yields. At low fluences the photolysis yield was found to be well below 1% and desorption of only one new photoproduct, HCl, was observed. At higher laser fluences, photolysis yields increase up to 5% and a significant fragmentation yield was reported. The ejection of additional photoproducts, namely Cl, $C_6H_4Cl_2$, $C_{12}H_9Cl$, $C_{12}H_{10}$ and $C_{12}H_8Cl$ were detected. It was also noticed that the phenyl products and HCl exhibited different velocity distributions.

In the present work, we perform a detailed comparison of the experimental data described above with a molecular-level picture emerging from the MD simulations. Verification of the model for a particular system is followed by a general discussion of the role of the laser-induced chemistry in the phenomena of UV laser ablation of molecular solids.

2. Computational setup

Our group has developed and applied an MD model to investigate the microscopic mechanisms of laser ablation [15–18,26]. In this model each molecule is represented by a single particle. In order to simulate molecular excitation by photon absorption and vibrational relaxation of the excited molecules, an additional internal degree of freedom is attributed to each molecule. The internal degree of freedom, or breathing mode, is accomplished by allowing the particles to change their sizes. The parameters of the inter-particle interaction are chosen to reproduce the properties of the material, whereas the parameters of the potential function ascribed to the internal degree of freedom are used to control the rate of the vibrational relaxation of the excited molecules. The approximate representation of the internal molecular motions permit a significant expansion of the time and length scales of the simulations and allows us to address collective effects in laser ablation. The full details of the breathing sphere model are given in Refs. [15,26].

Vibrational relaxation and photochemical fragmentation of the excited molecule are the dominant processes responsible for UV ablation. Previously, our group has examined laser ablation that occurs via vibrational relaxation of the excited molecules [15–18,26]. In this paper both of the possible results of photon absorption, namely photochemical fragmentation and vibrational relaxation of the excited molecule, are incorporated in the model. Vibrational excitation is modeled by depositing a quantum of energy equal to the photon energy into the kinetic energy of internal vibration of the excited molecule. Photochemical fragmentation is modeled by splitting up the excited molecule into fragments. These fragments have different masses, interaction potentials and sizes than the parent molecule and often occupy a larger volume, creating a local pressure inside the irradiated sample.

The laser irradiation at 248 nm wavelength is simulated by vibrational excitation or photochemical fragmentation of randomly chosen molecules during the 150 ps laser pulse. To reproduce the exponential attenuation of the laser light with depth the absorption probability is modulated by Beer's law with a laser penetration depth of 50 nm. In this case, the probability of a molecule to be excited depends on the laser fluence and the position of the molecule under the surface. In our calculations, most of the excited molecules undergo vibrational excitation, and only a certain percent of randomly chosen excited molecules can photofragment. Probability of photofragmentation can be defined based on the experimental observations of chlorobenzene in laser ablation [9].

The model of vibrational excitation is discussed in detail in our previous publications [15,17,26]. Below, we give a detailed description of photofragmentation model. The steps for incorporating photochemical events in the model are as follows:

- Pick a compound that has a well-known photochemistry.
- Identify possible reactions and products for the chosen compound.
- Choose potential parameters for the products from these reactions.
- Define reaction rates and probabilities.

The selection of chlorobenzene as our basic system for modeling photochemical events is based on the well-known photochemistry of the compound and extensive experimental studies that make a detailed interpretation/verification of the simulation results possible. A set of parameters is chosen to represent the chlorobenzene solid. To achieve a correct density of chlorobenzene (1.1064 g/cm^3), the equilibrium radius of the spherical particles representing these molecules

in the breathing sphere model is chosen to be 1.59 Å. The properties of model chlorobenzene solid such as sublimation energy of 0.612 eV, elastic bulk modulus of about 5 GPa, the calculated vibrational spectra are typical for organic solids.

To represent the photochemical processes in chlorobenzene, we chose reactions that are thermodynamically favorable and are observed in gas-phase or solution chemistry of chlorobenzene. The excited molecule undergoes a photodissociation reaction that produces two radicals, Ph–Cl → $Ph^{\bullet} + {}^{\bullet}Cl$ (Ph = phenyl). The radicals then react with chlorobenzene or other radicals by various abstraction and radical–radical recombination reactions. The complete list of the reactions induced by the laser excitation and subsequent photodecomposition of chlorobenzene in our model is given below.

Laser excitation of the molecule:

$$C_6H_5Cl + h\nu \rightarrow C_6H_5Cl^* \quad (1)$$

Photochemical fragmentation of the excited molecule:

$$C_6H_5Cl^* \rightarrow C_6H_5^{\bullet} + {}^{\bullet}Cl \quad (2)$$

Vibrational relaxation of the excited molecule:

$$C_6H_5Cl^* \rightarrow C_6H_5Cl \quad (3)$$

Abstraction reactions by primary radicals:

$$C_6H_5Cl + {}^{\bullet}Cl \rightarrow C_6H_4Cl^{\bullet} + HCl \quad (4)$$

$$C_6H_5Cl + C_6H_5^{\bullet} \rightarrow C_6H_4Cl^{\bullet} + C_6H_6 \quad (5)$$

$$C_6H_4Cl_2 + C_6H_5^{\bullet} \rightarrow C_6H_4Cl^{\bullet} + C_6H_5Cl \quad (6)$$

Radical–radical recombination reactions:

$$Cl^{\bullet} + {}^{\bullet}Cl \rightarrow Cl_2 \quad (7)$$

$$C_6H_5^{\bullet} + {}^{\bullet}C_6H_5 \rightarrow C_{12}H_{10} \quad (8)$$

$$C_6H_4Cl^{\bullet} + {}^{\bullet}C_6H_4Cl \rightarrow C_{12}H_8Cl_2 \quad (9)$$

$$C_6H_4Cl^{\bullet} + {}^{\bullet}C_6H_5 \rightarrow C_{12}H_9Cl \quad (10)$$

$$C_6H_4Cl^{\bullet} + {}^{\bullet}Cl \rightarrow C_6H_4Cl_2 \quad (11)$$

Abstraction reaction by secondary radical:

$$C_6H_5Cl + C_6H_4Cl^{\bullet} \rightarrow C_6H_5^{\bullet} + C_6H_4Cl_2 \quad (12)$$

For each reaction the standard heat of formation, $\Delta H_{rxn}{}^{\circ}$ (Table 1) is calculated from the available thermochemical data summarized in Table 2. When any of these reactions occur, the corresponding $\Delta H_{rxn}{}^{\circ}$ will be the amount of energy deposited into the system. In other words, the $\Delta H_{rxn}{}^{\circ}$ is the change in the total (potential plus kinetic) energy of the reaction products and the surrounding molecules. The amount of energy given off from each reaction is carefully monitored by adjusting initial positions of the reaction products and by performing additional local energy checks.

Obviously, from the above reactions, we need to choose a potential form to describe eight different molecules and three radicals. The pairwise additive potential among particles allows us to simulate multicomponent molecular systems without introducing additional specific potentials. The potential form is represented by the following formula

$$U_r = \varepsilon_n[\exp\{-2\alpha(r_{ij}{}^s - d_0)\} - 2\exp\{-\alpha(r_{ij}{}^s - d_0)\}],$$

where $r_{ij}{}^s$ is the distance between the edges of the particles, d_0 the equilibrium distance between particles, ε_n the potential well depth and α the anharmonicity constant. In this formulation, the intermolecular interaction depends on the distance between the edges of the breathing spheres rather than their centers. This definition is based on the physical concept that the sublimation or cohesive energy of an organic solid is governed primarily by the interactions among atoms on the outside of the molecule. In order to represent different organic molecules, we ascribe to each molecule an individual set of parameters (Table 2). For all molecules, the same equilibrium distance ($d_0 = 3.0$ Å) and anharmonicity constant ($\alpha = 1\,\text{Å}^{-1}$) have been chosen. In the potential between two different types of molecules, the well depth is calculated as the arithmetic mean of well depths of the corresponding molecules from Table 2. Because there is no available data on the sublimation energy of the radicals, parameters of the potentials between radicals and between radicals and molecules have been carefully fit to the values of the heat of reactions (Table 1). For example, the choice of the equilibrium radius, initial positions and parameters for the intermolecular potentials of Cl and C_6H_5 radicals is based on the value of the available energy for photofragments of 79.5 kJ/mol [13]. The potential between radicals has an equilibrium distance of 1.5 Å and anharmonicity constant equal to 1.1 Å. For the interaction between a radical and a molecule, a set of parameters ($d_0 = 2.5$ Å, $\alpha = 1.0\,\text{Å}^{-1}$, $\varepsilon_n = 0.05$ eV) is chosen. An internal degree of freedom is

Table 1
Heat of reactions (kJ/mol)[a]

	Reaction										
	(2)	(3)	(4)	(5)	(6)	(7)	(8)	(9)	(10)	(11)	(12)
$-\Delta H_{rxn}{}^{\circ}$(g)	79.5	482.7	109.3	144.9	146.7	239.2	478.9	194.0	410.9	248.5	35.2
$-\Delta H_{rxn}{}^{\circ}$(l)			66.4	136.5	144.6		555.4			294.0	34.6
$-\Delta H_{rxn}{}^{\circ}$(s)					119.7		564.4	282.3	410.9	318.9	

[a] Calculated from thermochemical data in Table 2 as $\Delta H_{rxn}{}^{\circ} = \sum \Delta H_f{}^{\circ}$ products minus $\sum \Delta H_f{}^{\circ}$ reactants. The designations g, l, and s represent data for gas, liquid and solid state reactions, respectively.

Table 2
Physical and thermochemical properties of molecules

Formula	Molecular weight (Da)	Melting point (°C)	Boiling point (°C)	Density (g/cm^3)	ε_n (eV)	Radii (Å)	$\Delta H_{f,298}{}^\circ$ (kJ/mol)	Ref.
C_6H_5Cl	112.56	−45	132	1.1064	0.1	1.58	54.42 (gas), 11.5 (liquid)	a,b,c
HCl	36.46	−114.8	−84.9	1.0004	0.069	1.086	(gas) −92.31	a,b,c
Cl_2	70.906	−100.98	−34.6	3.214	0.075	1.356	(gas) 0.0	a,b,c
C_6H_6	78.11	5.5	80.1	0.8787	0.122	1.4	(gas) 82.93 (liquid) 48.95	a,b,c
$C_6H_4Cl_2$(1,2-)	147.01	−17.0	179	1.3048	0.112	1.73	(gas) 33.0 (liquid) −17.4	a,b,c
(1,3-)		−25	172		0.109		(gas) 28.1 (liquid) −20.5	
(1,4-)		53	174		0.143		(gas) 24.6 (solid) −42.34	
$C_{12}H_{10}$	154.20	70.0	255.9	1.9896	0.15	1.76	(gas) 182.1 (liquid) 105.56 (solid) 96.73	a,b,c
$C_{12}H_9Cl$ (2-)	188.65	32.4	274.1	1.1499	0.134	1.88	(solid) 53.89	a,b,c
(3-)		16	284.5	1.1579	0.127			
(4-)		77.7	291.0		0.154		(solid) 76.595	
$C_{12}H_8Cl_2$ (4,4-)	223.1	148	315.9		0.185	1.99	(gas) 120.1	a,b,c
(2,2-)							(gas) 127.9	
(2,2-)							(solid) 31.7	
$C_6H_5{}^*$	77.102				0.05	1.39	330.5	a,c,d
Cl*	35.453				0.05	1.08	119.6	a,c,d
$C_6H_4Cl^*$	111.55				0.05	1.57	54.4	a,c,d

[a] Physical properties of molecules are taken from CRC Handbook of Chemistry and Physics, 58th Edition, CRC Press, Cleveland, OH, 1977.
[b] Thermochemical data for molecules are taken from NIST online databases at http://www.nist.gov/srd/online.html.
[c] Potential well depths, ε_n, are chosen to scale with the melting point of the compound. Radii of the molecules are calculated according to the density of the compound.
[d] Thermochemical data for radicals are taken from Y.H. Yim, M.S. Kim, J. Phys. Chem. 98 (1994) 5201.

attributed to each molecule that has a pyridine ring or other aromatic π-electron system because these systems can absorb a photon. Particles representing HCl, $Cl^\bullet$ and Cl_2 do not have the internal mode.

The choice of the dynamics and probabilities of the reactions is given and explained below. Generally, radical–radical recombination reactions are faster than abstraction reactions. Hence, the free chlorine, phenyl and chlorophenide ($C_6H_4Cl^\bullet$) radicals will try to react instantaneously with each other via reactions (7)–(11). If a radical does not encounter another radical during a certain time, t_l, then the radical can abstract a hydrogen or chlorine atom from the nearest chlorobenzene or dichlorobenzene molecule. The reactions will only take place if the radical finds a molecule or another radical within the certain distance equal to 3.0 Å. The choice of t_l for each radical is based on the concept that different radicals have different reactivities and lifetimes, and that the chlorine bond is weaker than the hydrogen bond in the molecule. The average lifetime of a radical is about 10^{-12} s [19]. In terms of reactivity, the chlorine radical is 2.7 times more reactive than phenyl radical and is about 3.1 times more reactive than chlorophenide radical [20]. The hydrogen abstraction reaction (4) will be, therefore, faster than hydrogen abstraction reaction (5). Thus we can assume that chlorine radical abstracts the hydrogen atom to form HCl molecule after $t_l = 0.3$ ps. After $t_l = 0.7$ ps, the phenyl radical looks for a dichlorobenzene molecule to abstract chlorine atom via reaction (6). If there is no dichlorobenzene around, it abstracts hydrogen atom from the nearest chlorobenzene molecule via reaction (5). The chlorophenide radical can abstract a hydrogen atom from the chlorobenzene molecule via reaction (12) after $t_l = 0.8$ ps only in the gas or liquid state.

In order to use a relatively large system with 126,950 molecules (10 nm × 10 nm × 191 nm), we employed a multiple step integration algorithm. The time step of 5 fs is used in the parts of the system where no reactions occur or no free radicals are present. In the regions where reactions are taking place, the time step is decreased to 0.5 fs. Dynamic non-absorbing boundary conditions are applied at the bottom of the sample to avoid artifacts due to the reflection of the laser-induced pressure wave from the edge of the computational cell [21]. Periodic boundary conditions in the direction parallel to the surface are imposed, simulating the conditions at the center of a laser spot.

3. Results and discussions

In the following section, the above model is applied for investigation of the role of the photofragmentation processes in 248 nm laser ablation of chlorobenzene films. We perform two series of MD simulations on the same sample for a range of laser fluences. In the first series, all of the excited molecules undergo vibrational relaxation with no photochemical reactions. In the second series, as suggested by experimental data [9], 5% of the excited molecules undergo photofragmentation. The fluence dependence of the molecular yields are compared and related to the difference in total deposited energy and average cohesive energy in these two systems. The influence of cohesive energy on the yield versus fluence dependence is discussed. The total amount of

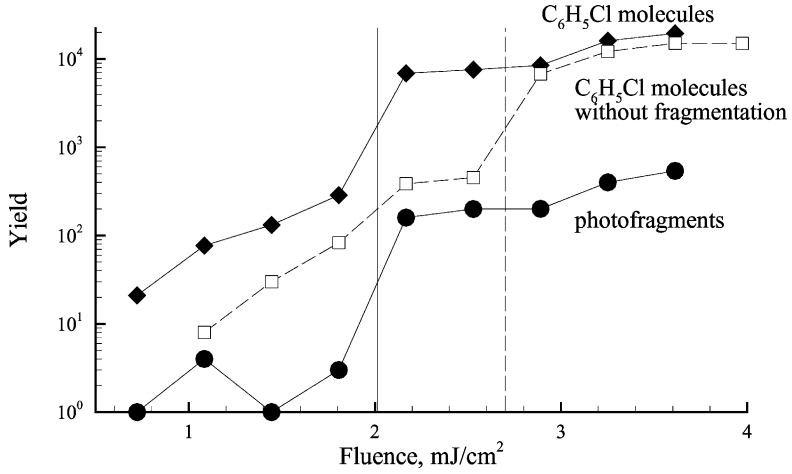

Fig. 1. Desorption intensities of molecular yields for the system with vibrational relaxation only (white squares and dashed line) and system with photochemical fragmentation as a function of laser fluence (solid lines). The gray diamonds and black circles represent the matrix and photofragment yields for the system with fragmentation. The vertical dashed and solid lines, respectively, mark the approximate position of the ablation thresholds.

photoproducts that form inside the sample with the corresponding photoproduct yields that are observed in clusters and monomers are then discussed and related to the experimental data.

The yields of molecules ejected from the first and second series of simulations upon laser irradiation are shown in Fig. 1. For both systems at a certain laser fluence, the yields sharply increase signifying the change in the ejection mechanism from desorption to ablation. In our simulations this increase of the molecular yield is coupled to the ejection of clusters of material and attributed to the ablation threshold [15–18,26]. For the system with photochemistry, at low fluences the ejection of the photoproducts is insignificant. The presence of reactions becomes visible only after the ablation threshold, where approximately 2% of the total yield is photoproducts. The reactions also affect the ablation threshold value that is lower in the system with photochemistry as compared to the system with vibrational relaxation only. Indeed, it was discussed by Tsuboi et al. [1,2] that, in the ablation of the liquid chlorobenzene sample the estimated temperature at the ablation threshold (97°C) is below the boiling point (132°C) signifying the contribution of photochemical fragmentation processes. Conversely, for benzene in which only vibrational relaxation of the molecules occurs, the estimated temperature is higher than the boiling point.

Analysis of the simulation results suggests that two effects are responsible for the decrease of the ablation threshold fluence as a result of introduction of photochemical reaction. One effect is the release of the additional energy from the exothermic reactions (Fig. 2(a)). Another effect is the overall weakening of the attractive interactions in the absorbing region due to the formation of volatile photoproducts (Fig. 2(b)). Below, we give an analysis of these two factors, starting with the effect of the reactions on the total energy deposited into the system.

The threshold difference is related to the difference in the total energy deposited into the systems (Fig. 2(a)). In the system without reactions, the energy deposited in the sample is directly defined by the laser fluence. In the case of the 248 nm irradiation, each photon absorbed increases the energy by 482.7 kJ/mol. In the simulations with photochemistry, the total energy has an additional contribution from the reactions. When the excited molecule undergoes fragmentation, most of the photon energy, 482.7 kJ/mol, goes to the bond rupture and the total energy only increases by 79.5 kJ/mol. Subsequently, the Cl radical can undergo an abstraction reaction (4), releasing 109.3 kJ/mol and forming chlorophenide radical. The latter can react with phenyl radical via reaction (10) with an additional release of 410.9 kJ/mol. The total energy in this scenario will increase by 599.7 kJ/mol, which is higher than the increase in energy caused by vibrational relaxation of the excited molecule. Thus the photochemical reactions increase the actual energy deposited by the laser pulse causing a shift of the ablation threshold to lower values.

Another factor that affects the threshold difference is the change of the attractive interactions in the absorbing region due to the presence of photoproducts. The results of our recent laser ablation study of systems with different cohesive energies suggest that the cohesive energy of the sample is related to the value of the ablation threshold [22]. The ablation threshold is defined by the critical energy density E_v^* required for the collective ejection of a volume of material or ablation [23,24]. It was shown that the threshold fluence $F^* = L_p E_v^*$ depends on the penetration depth L_p and the critical energy density E_v^*. The critical energy density is related to the binding energy of the organic solids and consequently, the ablation threshold should be the lowest for the system with the lowest cohesive energy. The fluence dependence of the total yield for three systems with different cohesive energies is shown in Fig. 3. The solid lines represent

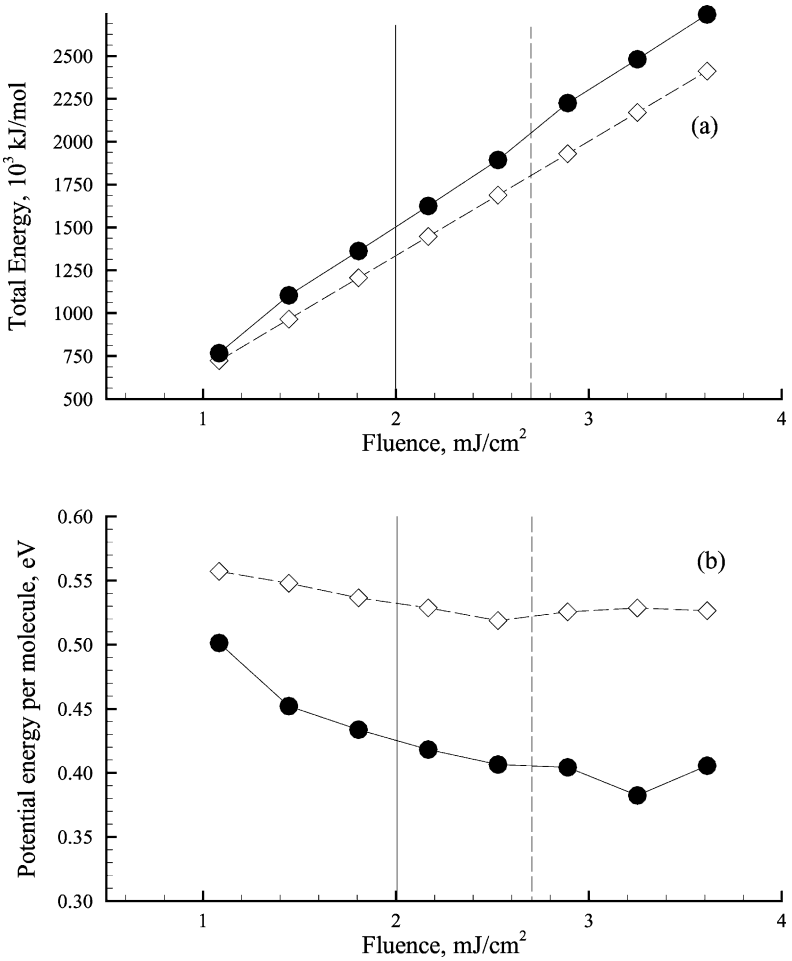

Fig. 2. Total deposited energy into the sample (a) versus laser fluence. Potential energy per molecule averaged over the top 30,000 molecules remaining in the sample after the ablation (b) versus laser fluence. White diamonds and dashed lines represent the system with vibrational relaxation only and black circles and solid lines represent the system with photochemical fragmentation of excited molecules.

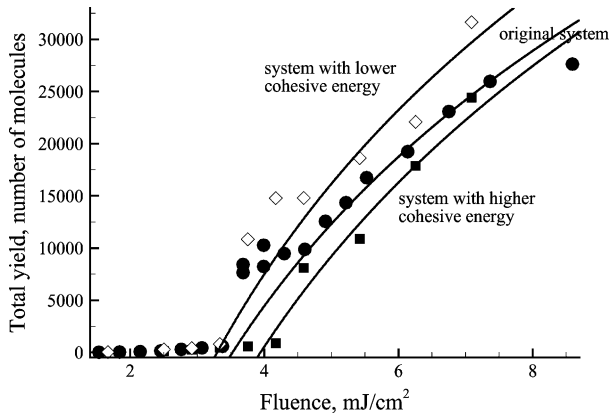

Fig. 3. Total yield versus fluence for three systems with different values of cohesive energy. The black circles represent the total yield from the original system with cohesive energy 0.6 eV and penetration depth 50 nm. The white diamonds and gray squares represent the total yield for the system with 0.57 and 0.66 eV cohesive energies, respectively, and penetration depth 55 nm. The solid lines represent prediction of the ablation model with critical energy density equal to 0.57, 0.60 and 0.66 eV, respectively.

the prediction of the ablation model given by the following equation

$$N_{\mathrm{tot}} = n_{\mathrm{m}} L_{\mathrm{p}} \ln\left(\frac{F}{L_{\mathrm{p}} E_{\mathrm{v}}^*}\right),$$

where n_{m} is the molecular number density of the material and N_{tot} the total number of ejected molecules. The cohesive energy of the original system is 0.6 eV [18], 0.57 eV for the system with lower cohesive energy, and 0.66 eV for the system with higher cohesive energy [22]. Even though for the two systems with modified cohesive energies the penetration depth is slightly higher (55 nm) than in the original system (50 nm), the assumption that the cohesive energy equal to the critical energy density is still valid.

The presence of volatile and non-volatile particles in the sample decreases or increases its average cohesive energy, respectively. In the present simulations, radicals HCl and Cl_2 are more volatile than chlorobenzene. Because the density of photofragmentation events follows Beer's law, there are more fragments present closer to the surface than deeper in

the sample. The presence of reactions and the number of photoproducts in the sample changes with time, hence it is difficult to calculate how reactions affect the cohesive energy of the sample. To highlight the effect of changing interactions in the surface region we have examined the sample after ablation and averaged the potential energy per molecule for the top 30,000 molecules remaining in the sample (Fig. 2(b)). Clearly, the presence of photoproducts in the sample significantly decreases the potential energy in the surface region in comparison to the simulations without fragmentation.

In the present study, the potential energy and the cohesive energy of the sample changes in time due to the presence of the photoproducts. The amount of photoproducts in the sample is controlled by reaction rates and probabilities. To illustrate this effect, the formation of photoproducts versus time at laser fluence equal to 2.9 mJ/cm^2 is shown in Fig. 4. During the laser pulse, the parent molecule breaks up into chlorine and phenyl radicals. The chlorine radical can react with other radicals via reactions (7) and (11) or abstract a hydrogen atom from the parent molecule via (4) forming a HCl molecule. The sharp rise of the concentration of volatile HCl during the laser pulse leads to the significant decrease of the potential energy in the absorbing region. No chlorine radical can be formed after the laser pulse and therefore, the concentration of HCl molecules reaches a steady state value. Approximately 74% of the HCl molecules never escape from the sample, even though the HCl molecule is nearly two times more volatile than the chlorobenzene molecule. Most of the phenyl radicals formed by photodissociation

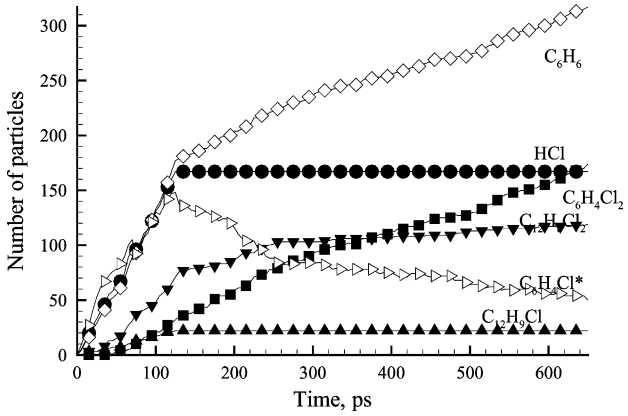

Fig. 4. Formation of photoproducts in time at laser fluence equal to 2.89 mJ/cm^2.

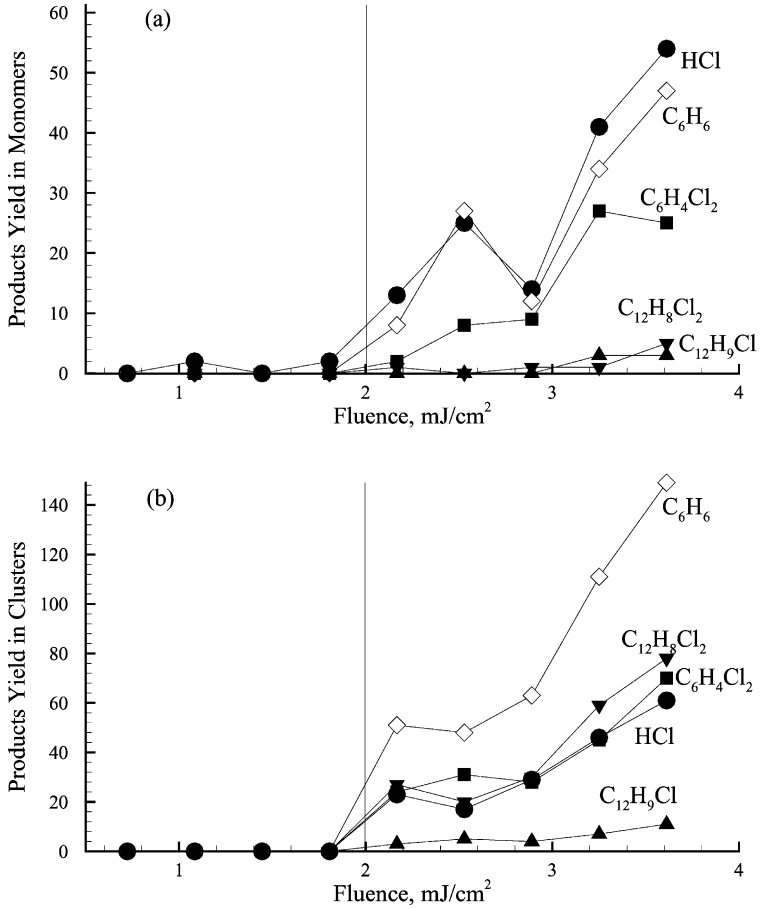

Fig. 5. Intensities of photofragments ejected in: (a) monomers or clusters less than four molecules and (b) clusters. Vertical lines indicate the approximate position of the ablation threshold.

participate in the formation of C_6H_6 molecules via reaction (5) and only a very small fraction undergoes reaction (10) to form $C_{12}H_9Cl$ molecules. In the present simulations, the probability of fragmenting the absorbing molecule (5%) is too small for the reactions (7) and (8) to occur. The increase of the $C_6H_4Cl^{\bullet}$ concentration during the laser pulse is dictated by reactions (4) and (5). This radical mostly reacts through reaction (9) forming $C_{12}H_8Cl_2$ molecules. Essentially, the tightly bounded biphenyls surround the HCl molecule and, therefore, it has very little chance to diffuse out of the sample unless it is formed near the surface. In the liquid and gas regions, the chlorophenide radical is responsible for the formation of $C_6H_4Cl_2$ and phenyl radicals via reaction (12). Reaction (12) increases the amount of phenyl radicals, consequently the concentration of benzene and $C_6H_4Cl_2$ rise after the laser pulse. Eventually, when all the $C_6H_4Cl^{\bullet}$ radicals react, the concentration profiles for all the products will be constant. The reactions involving phenyl and chlorophenide radical are slower than the chlorine radical abstraction reaction (4). Therefore, these radicals are present in the sample for a longer time than the chlorine radical. Thus, energy continues to be deposited into the system from reactions even after the laser pulse is over. After ablation, the majority of the photoproducts is trapped inside the sample. There are a total of 803 photoproducts formed at 650 ps, whereas only 201 are present in the plume.

One would expect from the data plotted in Fig. 4 to detect intensities of photoproducts in the plume in the following order: C_6H_6, HCl, $C_6H_4Cl_2$, $C_{12}H_8Cl_2$ and $C_{12}H_9Cl$. We have plotted the yield of ejected fragments in monomers and in clusters of less than four molecules (Fig. 5(a)) and the yield of fragments ejected as clusters (Fig. 5(b)). The relative ejection efficiency of different photoproducts can be explained based on the effect of the volatility of the species formed. We studied this effect in our previous study for a simple model system and found that volatile molecules eject mostly as monomers, whereas non-volatile molecules eject incorporated in clusters [22]. The results obtained in the present study are consistent with this observation. In the desorption regime only molecules that are more volatile than the matrix are ejected, which explains the presence of HCl in the plume below the ablation threshold. Above the ablation threshold, volatile HCl is the major photoproduct present as monomers. A significant fraction of benzene and dichlorobenzene molecules are also present in the plume as monomers, because they are only slightly less volatile than chlorobenzene. The non-volatile molecules $C_{12}H_9Cl$ and $C_{12}H_8Cl_2$ are ejected mostly incorporated into clusters. The presence of clusters is difficult to detect experimentally, and the monomer yield is usually detected. Our results for monomer ejection agree with experimental observation of chlorobenzene films [9,14,25] where HCl, $C_{12}H_{10}$, $C_6H_4Cl_2$, $C_{12}H_9Cl$, and $C_{12}H_8Cl_2$ were observed in the ablation regime. It was also noticed in experiment that the detection of C_6H_6 was hampered by the contribution of the strong $C_6H_5^+$ peak deriving from mass cracking of chlorobenzene.

4. Conclusions

In this paper, we have developed and applied a molecular-level model for investigation of the photofragmentation processes and their role in laser ablation of chlorobenzene films. We found that the presence of photofragmentation significantly lowers the ablation threshold value. Photofragmentation of molecules and following it reactions deposit additional energy into the sample even beyond laser irradiation. The presence of the reaction products in the sample lowers the potential energy and, consequently, cohesive energy of the sample in the absorption region. The yield of the photofragments becomes apparent only above the ablation threshold. Below the ablation threshold only volatile HCl was ejected. Even in the ablation regime most of the products stay trapped inside the sample. Hydrochloric acid, followed by benzene and dichlorobenzene are the main photoproducts ejected as monomers or as part of very small clusters. In addition, C_6H_6, $C_{12}H_8Cl_2$, $C_6H_4Cl_2$ and HCl are detected to be the main photoproducts that are ejected incorporated in clusters.

Acknowledgements

We acknowledge financial support from the Medical Free Electron Laser program of the office of the Naval Research and the Air Force Office of Scientific Research (AFOSR). In addition, the AFOSR provided support through the Multidisciplinary University Research Initiative program. The computational support was provided by the National Science Foundation through the MRI Program, the IBM through the Selected University Research Program and the Center for Academic Computing at Pennsylvania State University.

References

[1] Y. Tsuboi, K. Hatanaka, H. Fukumura, H. Masuhara, J. Phys. Chem. A 102 (1998) 1661.
[2] Y. Tsuboi, K. Hatanaka, H. Fukumura, H. Masuhara, J. Phys. Chem. 98 (1994) 11237.
[3] R. Srinivasan, A.P. Ghosh, Chem. Phys. Lett. 143 (1988) 546.
[4] M. Buck, P. Hess, Appl. Surf. Sci. 43 (1989) 358.
[5] K. Domen, T.J. Chung, J. Chem. Phys. 90 (1989) 3318.
[6] L.M. Cousins, S.R. Leone, Chem. Phys. Lett. 155 (1989) 162.
[7] G.C. Weaver, S.R. Leone, J. Phys. Chem. 100 (1996) 4188.
[8] R.J. Levis, C.J. Waltman, L.M. Cousins, R.G. Copeland, S.R. Leone, J. Vac. Sci. Technol. A 4 (1990) 3118.
[9] S. Georgiou, A. Koubenakis, M. Syrrou, P. Kontoleta, Chem. Phys. Lett. 270 (1997) 491.
[10] R.S. Davidson, J.W. Goodin, G. Kemp, Adv. Phys. Organic Chem. 20 (1984) 191, and references therein.
[11] T. Ichimura, Y. Mori, J. Chem. Phys. 58 (1973) 288.

[12] N. Ikeda, N. Nakashima, K. Yoshihara, J. Chem. Phys. 82 (1985) 5285.
[13] T. Ichimura, Y. Mori, H. Shinohara, N. Nishi, Chem. Phys. 189 (1994) 117.
[14] S. Georgiou, A. Koubenakis, J. Labrakis, M. Lassithiotaki, J. Chem. Phys. 109 (1998) 8591.
[15] L.V. Zhigilei, P.B.S. Kodali, B.J. Garrison, J. Phys. Chem. B 101 (1997) 2028.
[16] L.V. Zhigilei, P.B.S. Kodali, B.J. Garrison, Chem. Phys. Lett. 276 (1997) 269.
[17] L.V. Zhigilei, B.J. Garrison, J. Appl. Phys. 88 (2000) 1281.
[18] L.V. Zhigilei, B.J. Garrison, Appl. Phys. Lett. 74 (1999) 1341.
[19] M. Klessinger, J. Michl, Excited States and Photochemistry of Organic Molecules, VCH, USA, 1995.
[20] R.L. Huang, S.H. Goh, S.H. Ong, The Chemistry of Free Radicals, J.W. Arrowsmith Ltd., Bristol, UK, 1974.
[21] L.V. Zhigilei, B.J. Garrison, Mater. Res. Soc. Proc. 538 (1999) 491.
[22] Y.G. Yingling, L.V. Zhigilei, B.J. Garrison, A. Koubenakis, J. Labrakis, S. Georgiou, Appl. Phys. Lett. 78 (2001) 1631.
[23] R.E. Johnson, in: T. Baer, C.Y. Ng, I. Powis (Eds.), Large Ions: Their Vaporization, Detection and Structural Analysis, Wiley, New York, 1996, pp. 49–77.
[24] R. Srinivasan, B. Braren, Chem. Rev. 89 (1989) 1303.
[25] S. Georgiou, A. Koubenakis, J. Labrakis, M. Lassithiotaki, Appl. Surf. Sci. 127 (1998) 122.
[26] L.V. Zhigilei, P.B.S. Kodali, B.J. Garrison, J. Phys. Chem. B 102 (1998) 2845.